bioRxiv preprint doi: https://doi.org/10.1101/2022.07.06.498984; this version posted July 7, 2022. The copyright holder for this preprint (which was not certified by peer review) is the author/funder, who has granted bioRxiv a license to display the preprint in perpetuity. It is made available under aCC-BY-NC 4.0 International license.

A deep learning and graph-based approach to characterise the immunological landscape and spatial architecture of colon cancer tissue

Mario Parreno-Centeno[1], Guidantonio Malagoli Tagliazucchi[1], Eloise Withnell[1], Shi Pan[1], Maria Secrier[1,*]

[1]UCL Genetics Institute, Department of Genetics, Evolution and Environment, University College London, London, UK

[*]To whom correspondence should be addressed (m.secrier@ucl.ac.uk)

Running title: Integrated AI/graph-based analysis of colon cancer immunity

Keywords: colon adenocarcinoma, H&E slides, deep learning, cell-cell interaction graphs, tumour immunity, spatial transcriptomics, prognostic classifier

Financial support:

MPC was supported by an Academy of Medical Science Springboard award (SBF004\1042). GMT was supported by a Wellcome Seed Award in Science (215296/Z/19/Z). EW acknowledges the receipt of a studentship award from the Health Data Research UK-The Alan Turing Institute Wellcome PhD Programme in Health Data Science (Grant Ref: 218529/Z/19/Z). MS and SP were supported by a UKRI Future Leaders Fellowship (MR/T042184/1). Work in MS's lab was supported by a BBSRC equipment grant (BB/R01356X/1) and a Wellcome Institutional Strategic Support Fund (204841/Z/16/Z). For the purpose of Open Access, the author has applied a CC BY public copyright licence to any Author Accepted Manuscript version arising from this submission.

Corresponding author:

Maria Secrier
UCL Genetics Institute, London WC1E 6BT, UK
m.secrier@ucl.ac.uk

Conflict of interest:

The authors declare no potential conflicts of interest.

Word count: 4,360

Number of figures: 6

Number of tables: 0

bioRxiv preprint doi: https://doi.org/10.1101/2022.07.06.498984; this version posted July 7, 2022. The copyright holder for this preprint (which was not certified by peer review) is the author/funder, who has granted bioRxiv a license to display the preprint in perpetuity. It is made available under aCC-BY-NC 4.0 International license.

ABSTRACT

Tumour immunity is key for the prognosis and treatment of colon adenocarcinoma, but its characterisation remains cumbersome and expensive, requiring sequencing or other complex assays. Detecting tumour-infiltrating lymphocytes in haematoxylin and eosin (H&E) slides of cancer tissue would provide a cost-effective alternative to support clinicians in treatment decisions, but inter- and intra-observer variability can arise even amongst experienced pathologists. Furthermore, the compounded effect of other cells in the tumour microenvironment is challenging to quantify but could yield useful additional biomarkers. We combined RNA sequencing, digital pathology and deep learning through the InceptionV3 architecture to develop a fully automated computer vision model that detects prognostic tumour immunity levels in H&E slides of colon adenocarcinoma with an area under the curve (AUC) of 82%. Amongst tumour infiltrating T cell subsets, we demonstrate that CD8+ effector memory T cell patterns are most recognisable algorithmically with an average AUC of 83%. We subsequently applied nuclear segmentation and classification via HoVer-Net to derive complex cell-cell interaction graphs, which we queried efficiently through a bespoke Neo4J graph database. This uncovered stromal barriers and lymphocyte triplets that could act as structural hallmarks of low immunity tumours with poor prognosis. Our integrated deep learning and graph-based workflow provides evidence for the feasibility of automated detection of complex immune cytotoxicity patterns within H&E-stained colon cancer slides, which could inform new cellular biomarkers and support treatment management of this disease in the future.

bioRxiv preprint doi: https://doi.org/10.1101/2022.07.06.498984; this version posted July 7, 2022. The copyright holder for this preprint (which was not certified by peer review) is the author/funder, who has granted bioRxiv a license to display the preprint in perpetuity. It is made available under aCC-BY-NC 4.0 International license.

INTRODUCTION

Tumour immunity is a critical determinant of clinical outcome in colon adenocarcinoma[1,2], yet its characterisation is challenging due to cellular heterogeneity and the elaborate techniques required to study it comprehensively[3]. Earlier efforts introduced the prognostic value of the CD8+ to CD4+ T cell infiltration ratio within the tumour[4,5]. Galon et al[6] built on this to develop an 'Immunoscore' that predicts the risk of recurrence and chemotherapy response in colorectal cancer[7,8]. This score was derived based on immunohistochemistry (IHC), a fairly elaborate procedure to label antigens expressed by specific cells, which requires well defined markers and is not incorporated routinely in the clinical workflow. Instead, H&E staining of nucleus, cytoplasm and extracellular matrix offers a cheaper, streamlined alternative in oncology. Experienced pathologists can identify tumour infiltrating lymphocytes and other cells in H&E-stained tissue, but inter-and intra-observer variability can arise when assessing a sample[9]. Therefore, automating the detection of such cells could prove beneficial[10,11]. Indeed, deep learning algorithms have recently been employed for this purpose in multiple cancers[12-14], with links to patient outcome demonstrated in colorectal cancer[2,15].

However, these models often focus on individual cell types and do not consider the broader spatial organisation of the tissue, which can impact tumour growth and dissemination[16]. For instance, the stroma can promote tumour progression by limiting access of therapeutic agents or immune cells to tumours through fibrosis[17]. Such factors are currently challenging to assess systematically because of costs and a lack of standardised methodology. Several studies have shown that spatial organisation features such as the stromal content/ratios, TIL morphology and even immune hot/cold phenotypes can be extracted from H&E patches and linked to prognosis[12,18-23]. AbdulJabbar et al[24] and Bilal et al[25] have also integrated deep learning methods on digital histology and omics data more extensively, gaining insights into how cellular organisation impacts cancer evolution and clinical outcomes. However, these studies often require expert annotation and still lack insight into more complex interactions between different cell types.

bioRxiv preprint doi: https://doi.org/10.1101/2022.07.06.498984; this version posted July 7, 2022. The copyright holder for this preprint (which was not certified by peer review) is the author/funder, who has granted bioRxiv a license to display the preprint in perpetuity. It is made available under aCC-BY-NC 4.0 International license.

As an alternative to expert annotation, developments of computational tools for immune deconvolution from RNA sequencing have revolutionised our ability to capture an extensive array of cell types and states in bulk tissue[26-28]. Cancer transcriptomics datasets are widely available and have been successfully integrated with H&E images via deep learning in recent studies, demonstrating that patterns of angiogenesis, hypoxia and even T and B cell immunity are detectable in the tissue[29]. Integrating such approaches to characterise tumour immunity as a whole within the colon cancer tissue would be highly informative for prognosis and treatment, but has not yet been achieved.

This study tests the extent to which tumour immunity and its spatial organisation can be quantified within colon adenocarcinoma tissue based on transcriptomic signatures alone. We propose a fully automated image-processing pipeline to predict the immune activity in a tumour from H&E images based on matched bulk RNA-seq data. We also introduce a novel framework for surveying detailed cellular interaction landscapes within digital pathology slides by combining nuclear segmentation, classification and graph assembly, with efficient queries handled via a bespoke Neo4J graph database. Finally, we apply this framework to interrogate the complex tissue organisation in colon adenocarcinoma and identify cellular structures linked with immune response, which we then validate using spatial transcriptomics.

RESULTS

Transcriptome-derived tumour immunity informs prognosis, molecular characteristics and treatment efficacy in colon adenocarcinoma

To explore the immune landscape and tissue organisation of colon adenocarcinoma, we employed RNA sequencing (RNA-seq) and matched digital pathology data collected from tumour samples of 456 patients available from TCGA. We calculated a tumour immunity score per sample as the

bioRxiv preprint doi: https://doi.org/10.1101/2022.07.06.498984; this version posted July 7, 2022. The copyright holder for this preprint (which was not certified by peer review) is the author/funder, who has granted bioRxiv a license to display the preprint in perpetuity. It is made available under aCC-BY-NC 4.0 International license.

average abundance of tumour infiltrating cells from the microenvironment using ConsensusTME[28] (Supplementary Figure 1a). This score accounted for the compounded effects of expression signals coming from all detectable non-tumour cells, reflecting a spectrum of low to high immunity (Supplementary Figure 1b). The score correlated well with the mean CD8+/CD4+ T cell subtype scores estimated from transcriptomic data using an alternative immune deconvolution method, xCell ($R = 0.46$, $p<2e-16$).

After quantifying the overall tumour immunity in each sample, we assessed the prognostic value of the respective immune scores. To maximise the clinical relevance of this analysis, we sought to identify a tumour immunity score threshold that would reflect the strongest relation with patient outcome. We found that a cut-off point of 0·39 highlighted two immunity groups (High Immunity, HI, and Low Immunity, LI) with highly distinct overall survival ($p=0·002$, Figure 1b-c) and disease-free intervals ($p=0·005$, Supplementary Figure 1c). As expected, the patients with high levels of tumour immunity showed significantly better outcomes. When checking against the pathology annotations of the slides, the differences between the HI and LI groups appeared to be driven by the presence of lymphocytes and neutrophils, which were elevated in the HI group (Figure 1d). Furthermore, the HI tumours also had elevated markers of intratumoural natural killer (NK) cell activity, including expression of NK cell receptors and corresponding tumour cell ligands, as well as secreted cytokines (Supplementary Figure 1d), which have been associated with immunotherapy response[30].

Colon cancer has been systematically characterised from a genomic point of view, with mutation, expression and methylation features shown to associate with disease progression and therapy responses[31,32]. To link these findings with our classification, we further characterised the 456 samples in the HI/LI groups using molecular and tumour architecture phenotypes already described for colon adenocarcinomas[31] (Figure 1e). Genomically, we found that low immunity tumours tended to fall within the chromosomally unstable group of gastrointestinal cancers (CIN). Indeed, tumours with higher levels of CIN/aneuploidy have been previously linked with immune

bioRxiv preprint doi: https://doi.org/10.1101/2022.07.06.498984; this version posted July 7, 2022. The copyright holder for this preprint (which was not certified by peer review) is the author/funder, who has granted bioRxiv a license to display the preprint in perpetuity. It is made available under aCC-BY-NC 4.0 International license.

evasion and poorer outcomes to immunotherapies[33]. In contrast, high immunity tumours were associated with the gastrointestinal hypermutated indel (HM-indel) subtype and presented frequent microsatellite instability (MSI), in line with numerous studies linking hypermutation with increased neoantigen presentation and activation of the host antitumor immune response[34,35].

The consensus expression-based classification defined by Guinney et al[32] revealed that the high immunity tumours tended to be more mesenchymal (CMS4), a subtype characterised by increased stromal infiltration and angiogenesis. In contrast, lower immunity was linked with epithelial, metabolically deregulated phenotypes (CMS2/3), and lacked the characteristic pattern of CpG island hypermethylation (non-CIMP). Anatomically, low immunity was more frequently characteristic of tumours arising in the descending colon and on the left side, and prevailed in late-stage cancers, where immune recognition is more likely impaired. Tumours with higher immunity tended to present fewer hyperplastic polyps.

Finally, the two defined immunity groups in colon adenocarcinomas were predicted to display significantly different susceptibility to multiple anti-cancer compounds (Figure 1f). The largest differences were observed for chemotherapy drugs such as topotecan, mitoxantrone and gemcitabine. Higher immune activity was linked with lower IC50 values, suggesting greater efficacy in this setting and confirming previous links between immunity and enhanced chemotherapeutic responses[8].

A prognostic classifier of tumour immunity in colon cancer from H&E-stained images

Having demonstrated the clinical relevance of our immune classification of colon adenocarcinomas, we then developed a digital pathology classifier of this phenotype. We trained a deep learning model based on the InceptionV3 architecture to classify high and low tumour immunity (as inferred from matched RNA-seq data) in H&E-stained images of cancer tissue collected from colon adenocarcinoma patients (Figure 2a). We achieved a median accuracy of

bioRxiv preprint doi: https://doi.org/10.1101/2022.07.06.498984; this version posted July 7, 2022. The copyright holder for this preprint (which was not certified by peer review) is the author/funder, who has granted bioRxiv a license to display the preprint in perpetuity. It is made available under aCC-BY-NC 4.0 International license.

82% AUC probability based on tile average and percentage count in the testing dataset (Fig 2b-c). This approach also allowed us to obtain a spatially-resolved overview of tumour immunity levels within entire tissue slides through tile-level estimates (Fig 2d). Indeed, tissue slides from highly immunogenic tumours were predominantly composed of tiles with strong HI signals, whereas low immunity tumours presented more diverse predictions of LI and intermediate levels of immunity across tiles (Fig 2e).

While the HI group of tumours is expected to have enhanced immune reactivity, the cytotoxic effect is triggered by populations of CD8+ and CD4+ immune cells that are transformed from a naïve to an effector state upon antigen recognition[36]. These CD8+/CD4+ subsets emerge at different points of cancer development and could create distinct patterns within the tumour tissue. The ability of deep learning algorithms to distinguish these immune subsets in H&E slides has not been tested in this system. To understand whether patterns of active rather than uneducated immunity might be preferentially captured, we trained deep learning models to identify distinct subgroups of CD4+ and CD8+ T cells as characterised in Aran et al[27], i.e., CD4/CD8+ naïve T cells, central memory cells and effector memory cells in the TCGA COAD cohort. Our models could detect expression signals of CD4+ central memory T cells and CD8+ effector memory T cells with high accuracies of 82% and 83% AUC, respectively (Figure 3). The rest of the cells were identified with lower accuracy, between 64% and 70% AUC. Overall, this suggests that the cells most relevant to triggering an effective immune response are also the ones that leave the most recognisable traces within the colon cancer tissue and could be specifically tracked in a clinical setting to support immunotherapy treatment decisions.

Cellular organisation of the immune response in colon adenocarcinoma

Next, we sought to gain further insight into the cellular organisation of colon adenocarcinoma tissue in a high versus low immunity setting using the H&E slide information. Using HoVer-Net[37], we conducted nuclear segmentation and classification within the H&E tiles of the TCGA

bioRxiv preprint doi: https://doi.org/10.1101/2022.07.06.498984; this version posted July 7, 2022. The copyright holder for this preprint (which was not certified by peer review) is the author/funder, who has granted bioRxiv a license to display the preprint in perpetuity. It is made available under aCC-BY-NC 4.0 International license.

179 COAD dataset. This approach allowed us to label individual cells within the tissue as 'tumour',
180 'lymphocytic' or 'stromal' (Figure 4a). Based on cell proximity, we could then infer interactions
181 between different cells and summarise them for every tissue patch in the form of graphs (Figure
182 4a). However, this analysis resulted in thousands to hundreds of thousands of interactions per
183 sample, yielding complex graphs that are difficult to store, integrate and query. To resolve this,
184 we developed a Neo4J graph database comprising 2,786,464 nodes and 3,628,377 edges, that
185 would allow us to explore and interrogate such complex structures effectively. The basic
186 relationship model in the database is depicted in Figure 4b. This database allows us to perform
187 complex queries to identify biologically relevant structures, such as a stromal barrier separating
188 lymphocytes from tumour cells (Figure 4c), or a lymphocytic attack on cancer cells (Figure 4d).
189 These graph interactions can also be dynamically explored and expanded within the database
190 (Supplementary Video 1).

191 We compared the cell population frequencies and interactions between the HI and LI groups.
192 Lymphocytes and stromal cells were similarly abundant in the two groups, but appeared more
193 frequently isolated in a high immunity context (Figure 5a-b). These could correspond to exhausted
194 or naïve T cells being recruited to the site, which would be less likely to form interactions. As
195 expected, the HI group also harboured more frequent direct interactions between lymphocytes and
196 tumour cells, suggesting immune recognition typical of 'immune hot' phenotypes[38] (Figure 5c,e).
197 The number of tumour-stroma interactions was also increased (Figure 5d), but to a lower extent
198 (Figure 5e). On the other hand, dense lymphocyte clusters in the form of triplets, as well as stromal
199 barriers were increased in the low immunity tumours (Figure 5f-g). The lymphocyte triplet
200 presence might suggest inactive clusters that are not recognising malignant cells. Concurrently,
201 the stromal barriers may aid immune evasion, as has been previously described in pancreatic
202 cancer[39]. These cellular structures reflect different cellular organisation and immune activity in
203 an HI vs LI setting and could support treatment strategies in the clinic.

bioRxiv preprint doi: https://doi.org/10.1101/2022.07.06.498984; this version posted July 7, 2022. The copyright holder for this preprint (which was not certified by peer review) is the author/funder, who has granted bioRxiv a license to display the preprint in perpetuity. It is made available under aCC-BY-NC 4.0 International license.

Validation of deep learning predictions using spatial transcriptomics

Finally, to validate our model predictions using an orthogonal approach, we employed spatial transcriptomics data available for one colorectal tissue slide from the Visium platform (Figure 6a). We applied our AI model on the H&E stained image to obtain predictions of the overall immunity within the tumour at patch level (Figure 6b). In parallel, we analysed the spatial gene expression profiles across multiple spots within the image and derived an immunity map outlining the distribution of immune 'hot' and 'cold' islands across the tissue (Figure 6c-d).

By visually comparing the AI model predictions with the spatial profile, we can see there is a good agreement between the two methods (Figure 6b-d). In particular, it is striking that the central area of high immunity (island 1) appears as a diagonal stripe both in the spatial transcriptomics as well as in our model's predictions, with smaller islands of increased immunity present to the left and right of this region (islands 2-4, Figure 6b-c). The immune 'hot' areas presented marked CMS4 features, while the colder areas more frequently contained CMS1/2/3 types of cells (Supplementary Figure 2a-d), as previously shown in the bulk data.

When reconstructing cell-cell interactions within the spatially profiled slide, we confirmed an increase in epithelial-lymphocyte interactions in the immune 'hot' compared to the immune 'cold' areas (20% versus 5%). Furthermore, interactions between stromal cells and lymphocytes appeared confined to the immune hot regions (41%), with no stromal cells detected in the immune cold areas. The CD8+ and CD4+ T cell spatial structure was very similar in the immune cold regions, with larger interaction modules observed in the immune hot regions (Figure 6e). The immune hot regions were denser, with CD8+ and CD4+ T cell graphs having a density metric of 0.095 and 0.073 respectively, and immune cold regions with a density metric of 0.046 and 0.0451. Immune hot CD8+ and CD4+ graphs also presented increased connectivity (12 connected components each versus 30 and 31 connected components in immune cold regions, respectively).

bioRxiv preprint doi: https://doi.org/10.1101/2022.07.06.498984; this version posted July 7, 2022. The copyright holder for this preprint (which was not certified by peer review) is the author/funder, who has granted bioRxiv a license to display the preprint in perpetuity. It is made available under aCC-BY-NC 4.0 International license.

As expected, the high immunity areas also presented increased CD8/CD4+ T cell and stromal cell abundance, while containing fewer NK cells (Figure 6f, Supplementary Figure 2e-f).

All these point towards the co-existence of immune hot and cold areas within tumours that display distinct spatial interactions and confirm many of the features we were able to capture through our deep learning and graph models. While this analysis is limited by the availability of a single slide, it serves as a proof of concept that H&E-based deep learning models could be validated using spatial transcriptomics.

DISCUSSION

In this work, we have employed state-of-the-art methodology to establish an RNA-seq-derived immune signature in colon adenocarcinoma that is prognostic and links with differential efficacy of various chemotherapeutics. We have shown that this signature is detectable in H&E-stained colon cancer tissue. Furthermore, we have introduced novel methods to explore the ample space of cellular interactions underlying distinct tumour immunity phenotypes, unveiling specific rewiring that could inform diagnosis and treatment.

The encouraging performance of 82% for our tumour immunity classifier in H&E images suggests that integrating such images and transcriptomics data could support faster pathology annotation and triage in a setting where this staining procedure is routine. Our model's performance was similar to that of other methods assessing immunity-linked phenotypes like MSI, mutability or methylation status in colorectal cancer[25], and outperformed immune classification/immunotherapy response models in breast cancers[40] and melanoma[41] with AUCs of 76-78%. It is worth noting that multiple studies have applied deep learning for lymphocyte feature extraction in colorectal cancer and linked this with outcome[42,43]. However, these fall short of providing a direct H&E-based classifier. While our model does not outperform MSI classifiers developed in this cancer[44,45], it captures a different and more versatile phenotype of tumour

bioRxiv preprint doi: https://doi.org/10.1101/2022.07.06.498984; this version posted July 7, 2022. The copyright holder for this preprint (which was not certified by peer review) is the author/funder, who has granted bioRxiv a license to display the preprint in perpetuity. It is made available under aCC-BY-NC 4.0 International license.

immunity. It also helps us explore the limits of prognostic classification based on expression-derived signatures, for which datasets are much more widely available.

We also showed that not all T cells associated with the antitumour immune response are equally detectable in the cancer tissue when trained on expression markers. This could be due to morphological confounders or to the expression signatures not being specific enough for some cell types. Nevertheless, the cells effectively responsible for cytotoxicity (effector CD8+ and central memory CD4+ T cells) presented the best classification performance, suggesting that both short-term and longer-term immune stimulation may be captured.

Our investigation of the cellular organisation of the tissue has highlighted niche structures such as dense lymphocyte clusters/triplets, or stromal barriers which may account for the lack of immune recognition and worse prognosis in the low immunity group, as reported by other studies too[18,46]. This showcases the importance of spatial analysis of the tumour microenvironment to understand cancer progression. A limitation is that the cell types identified are rather generic. Improved methods are needed in the future to distinguish diverse cell populations, e.g. cancer-associated fibroblasts, T and B cell subsets, and gain a finer-grained resolution of the landscape of cell-cell relations established. Moreover, the structures studied here should be further investigated experimentally to clarify the mechanism by which they contribute to immune evasion. Finally, our spatial transcriptomics validation illustrates one key factor that needs to be built into such models in the future: the spatial heterogeneity of immune hot/cold phenotypes. Future studies should focus on integrating deep learning on H&E slides, spatial transcriptomics models and graph reconstruction methods to obtain a spatially-informed predictor of tumour immunity and response to therapies.

This study proposes a prognostic classifier for tumour immunity in colon adenocarcinoma with distinct tumour and microenvironment architecture features. While we have based our classifier on expression rather than protein-level/IHC data, our immune signature is nevertheless highly

bioRxiv preprint doi: https://doi.org/10.1101/2022.07.06.498984; this version posted July 7, 2022. The copyright holder for this preprint (which was not certified by peer review) is the author/funder, who has granted bioRxiv a license to display the preprint in perpetuity. It is made available under aCC-BY-NC 4.0 International license.

prognostic and many of its features are recapitulated in spatial transcriptomics data. It thus could be valuable in the clinic as additional support for treatment decisions. Most importantly, we propose a novel integrative approach to digital pathology analysis in cancer, combining H&E-stained slides and matched RNA-seq data through deep learning, and making use of the capabilities of the Neo4J graph database methodology to efficiently quantify and explore tissue landscapes and cellular interactions. This framework enables a faster, more extensive and more interpretable exploration of key immunity features than with traditional approaches, and could be easily adapted to answer a variety of biological questions in cancer as well as healthy tissue settings.

MATERIALS AND METHODS

Molecular data sources and immune stratification

RNA-seq data from 456 colon adenocarcinoma (COAD) tumours, along with clinical and pathology information, were retrieved from The Cancer Genome Atlas (TCGA) using the *TCGAbiolinks* R package. No samples were excluded based on demographics criteria. We estimated the relative abundance of various lymphoid and myeloid cell subsets, endothelial cells and fibroblasts (Supplementary Table 1) based on the expression of cell type-specific markers using ConsensusTME[28]. The 'immunity score' was defined as the average abundance across all cell types within a sample, as in the original study (Supplementary Figure 1a). This score was used to stratify the cohort into two groups representing low and high immunity. For this, we used the threshold that maximises the difference in overall survival between the high/low immunity groups, i.e. testing different thresholds by sequentially increasing their value using the *survminer* R package.

bioRxiv preprint doi: https://doi.org/10.1101/2022.07.06.498984; this version posted July 7, 2022. The copyright holder for this preprint (which was not certified by peer review) is the author/funder, who has granted bioRxiv a license to display the preprint in perpetuity. It is made available under aCC-BY-NC 4.0 International license.

299 xCell[27] expression-based estimates of CD8+ and CD4+ naïve, central and effector memory T cell
300 populations were obtained for all TCGA COAD cancers from https://xcell.ucsf.edu/ . The cohort
301 was split by the mean infiltration estimate of each CD8/CD4+ T cell population.

302 Signatures of intratumoural NK cell activity were assessed based on the expression of NK cell
303 receptors, tumour ligands and cytokines as detailed in Huntington et al[30]. An expression score
304 summarising these activities was defined per sample using single sample Gene Set Enrichment
305 Analysis via the *GSVA* R package.

306 We derived the molecular phenotypes of colorectal cancer from Liu et al[31] and Guinney et al[32],
307 and retrieved the predicted drug sensitivity IC50 values for TCGA samples from Li et al[47].

308 **Image pre-processing**

309 A total of 874 images of H&E-stained tissue collected from 456 COAD patients were obtained
310 from the TCGA Genomic Data Commons Data Portal (GDC Data Portal) (RRID:SCR_014514,
311 https://portal.gdc.cancer.gov/). Because of the high resolution and large scale of these images, a
312 common pre-processing method before applying deep learning approaches for the classification
313 of whole slide images (WSIs) is to crop them into small sections called tiles[64]. We extract all
314 possible non-overlapping tiles following a grid structure and we filter those including more than
315 50 percent of background. We set the size of the tile to 512px by 512px, yielding a total of more
316 than 2 million of them, which were then used to train and test our model (described below).

317 To avoid inconsistencies in the preparation of histology slides arising from dye concentration,
318 duration of staining and temperature differences[48], we employed StainTools
319 (https://pypi.org/project/staintools/) to normalize each H&E patch used in this study. The stain
320 matrix estimation was set to be calculated via the Vahadane method.

321

bioRxiv preprint doi: https://doi.org/10.1101/2022.07.06.498984; this version posted July 7, 2022. The copyright holder for this preprint (which was not certified by peer review) is the author/funder, who has granted bioRxiv a license to display the preprint in perpetuity. It is made available under aCC-BY-NC 4.0 International license.

H&E-based classifier of tumour immunity

To classify immunity levels in H&E images, we used a model consisting of two parts: a convolutional neural network (CNN) feature extractor followed by a non-linear classifier (Figure 2a). We based the feature extractor backbone in the InceptionV3 architecture[43]. First, we resized the 512x512px tiles with three colour channels to 299x299px, as this is the required input size of the model. Furthermore, we scaled the input pixel values that were initially in the range of (0;255) to a range of (-1;1).

We removed the top layer of the InceptionV3 original architecture, and used the bottleneck layer's feature representation. This converts each input image of size 299x299x3 into an 8x8x2,048 block of features. Here, we average over the 8x8 spatial locations, using a Global Average Pooling 2D layer to convert the block of features to a single 2,048-element vector per image. We feed this vector image to a fully connected classifier to convert these features into a single prediction per image. It consists of two dense layers of 1,024 and 512 units, respectively, with a RELU activation function. We applied a dropout regularisation to the output of the first dense layer. Low immunity samples are predicted as class 0 and high immunity as class 1.

We initialised the parameters of the InceptionV3 layers with weights trained in the ImageNet dataset[49]. To avoid destroying the pre-loaded weights, we trained the full model end-to-end with a small learning rate (1e-5). In this way, we fine-tuned the higher-order feature representations in the base model to make them more relevant for this task. During the training, we introduced sample diversity by applying random transformations to the input images, such as rotation, shearing, zooming, horizontal and vertical flipping. To avoid overfitting, we applied L2 regularisation to the kernel of the 2D convolutional layers of the InceptionV3 model during the optimisation. We added this penalty to the loss function as the sum of the squared weights.

We used 70% of the samples for training and 30% for testing, undersampled to the lower class. We repeated each experiment five times with different chosen random samples for training and

bioRxiv preprint doi: https://doi.org/10.1101/2022.07.06.498984; this version posted July 7, 2022. The copyright holder for this preprint (which was not certified by peer review) is the author/funder, who has granted bioRxiv a license to display the preprint in perpetuity. It is made available under aCC-BY-NC 4.0 International license.

testing. To present the results, we show the Receiver Operating Characteristic (ROC) curve and the Area Under the Curve (AUC) for each experiment and the total average for all the cross-validation splits.

Graph-based reconstruction of cell-cell interactions

We used the HoVer-Net computational pathology pipeline trained on the CoNSeP dataset[37] to segment and classify nuclei within H&E-stained tiles into four categories depending on cell type: tumour cells, lymphocytes, stroma and miscellaneous cells. The miscellaneous category groups artefacts or ambiguous cell types e.g. necrotic, mitotic cells and others that cannot be categorised. This category was discarded from further analysis.

The identified nuclei and their positioning within the tissue were used to reconstruct and analyse the spatial interactions between cells. Each nucleus/cell was represented by a node in a graph. We determined interactions between cells based on spatial proximity, with any two cells situated <35 µm apart assumed to be interacting[50]. We assigned an edge between adjacent cells, depicting the interaction. We then employed the Neo4J Graph Database framework (https://neo4j.com/) to store and efficiently query the graphs derived from the WSIs of 110 patients belonging to either the high or low tumour immunity class.

We compared the cell type abundance and the frequency of different interactions between the high and low immunity groups. A *stromal barrier* was defined as an instance where lymphocytes can reach a tumour cell by crossing a stromal cell in each sample. *Lymphocyte triplets* were defined as three lymphocyte cells sequentially connected. We normalised the number of stromal barriers by the sample's total number of stromal-stromal relations. Similarly, we normalised lymphocyte triplets by the sample's total number of lymphocyte-lymphocyte relations.

bioRxiv preprint doi: https://doi.org/10.1101/2022.07.06.498984; this version posted July 7, 2022. The copyright holder for this preprint (which was not certified by peer review) is the author/funder, who has granted bioRxiv a license to display the preprint in perpetuity. It is made available under aCC-BY-NC 4.0 International license.

Spatial transcriptomics data analysis

The human colorectal cancer patient sample was downloaded from 10x genomics (https://support.10xgenomics.com/spatial-gene-expression/datasets). The output from the Space Ranger Visium pipeline was used for analysis. The *SCTransform* R package was used to normalise the data using a regularised negative binomial regression method. The *Seurat* R package was used to calculate and visualize the gene module scores across the slide. Immunity was scored for each spot using the ConsensusTME methodology. Independently, cell type and state proportions for each spot were estimated using the DestVI package. DestVI requires scRNA from the same tissue for deconvolution. 18,409 cells from 2 colorectal patients were downloaded from Lee et al[51]. The major cell types consisted of B cells, T cells, Epithelial cells, Mast cells, Myeloids and Stromal cells, consistent with the HoVer-Net cellular deconvolution categories. To further break down the cellullar categories, we also used the minor class labels for CD19+CD20+ B, CMS1, CMS2, CMS3, CMS4, IgG+ Plasma, Lymphatic ECs, Myofibroblasts, NK cells, Proliferative ECs, Smooth muscle cells, Stromal 1, Stromal 2, T follicular helper cells, T helper 17 cells, Tip-like ECs, cDC cells as labels. Scanpy[52] (Single-Cell Analysis in Python) and Squidpy[53] (Spatial Single Cell Analysis in Python) packages were used for graph analysis. This included graph visualisation and graph metric algorithms. Immune hotspots were calculated from the immune score signature using PySAL (Python Spatial Analysis Library) and separate immune cold and immune hot graphs were calculated from these immune hotspot regions.

Statistics

Cell organization and disease characteristics were compared between groups using the Wilcoxon rank-sum test. The association between immunity groups and patient outcomes was evaluated using Cox proportional hazards models.

bioRxiv preprint doi: https://doi.org/10.1101/2022.07.06.498984; this version posted July 7, 2022. The copyright holder for this preprint (which was not certified by peer review) is the author/funder, who has granted bioRxiv a license to display the preprint in perpetuity. It is made available under aCC-BY-NC 4.0 International license.

Data availability

The results published here are based in part upon publicly available data generated by the TCGA Research Network (https://www.cancer.gov/tcga). All these data comply with ethical regulations, with approval and informed consent for collection and sharing already obtained by the TCGA consortium.

The spatial transcriptomics data employed in the study was freely available for reuse from 10x Genomics through the Visium platform (https://support.10xgenomics.com/spatial-gene-expression/datasets).

Ethical approval and written informed consent were not required for this study.

Code availability

The code developed for the purpose of this study can be found at the following repository: https://github.com/secrierlab/TumourHistologyDL

AUTHOR CONTRIBUTIONS

MS designed the study and supervised the analyses. MPC built the deep learning classifiers, performed the nuclear segmentation and classification, built the Neo4J graph database and analysed the interactions in HI and LI tumours. GMT and MPC developed the immunity signatures. GMT and MS performed associations with molecular subtypes of colorectal cancer, and further interaction analyses. EW performed the spatial transcriptomics analysis. SP performed the Visium slide TIFF image conversion and pre-processing. All authors wrote and approved the manuscript.

bioRxiv preprint doi: https://doi.org/10.1101/2022.07.06.498984; this version posted July 7, 2022. The copyright holder for this preprint (which was not certified by peer review) is the author/funder, who has granted bioRxiv a license to display the preprint in perpetuity. It is made available under aCC-BY-NC 4.0 International license.

REFERENCES

1. Lavotshkin, S. *et al.* Immunoprofiling for prognostic assessment of colon cancer: a novel complement to ultrastaging. *J Gastrointest Surg* **19**, 999-1006 (2015).
2. Galon, J. *et al.* Type, density, and location of immune cells within human colorectal tumors predict clinical outcome. *Science* **313**, 1960-4 (2006).
3. Jamal-Hanjani, M., Thanopoulou, E., Peggs, K.S., Quezada, S.A. & Swanton, C. Tumour heterogeneity and immune-modulation. *Curr Opin Pharmacol* **13**, 497-503 (2013).
4. Hernberg, M., Muhonen, T., Turunen, J.P., Hahka-Kemppinen, M. & Pyrhönen, S. The CD4+/CD8+ ratio as a prognostic factor in patients with metastatic melanoma receiving chemoimmunotherapy. *J Clin Oncol* **14**, 1690-6 (1996).
5. Diederichsen, A.C., Hjelmborg, J., Christensen, P.B., Zeuthen, J. & Fenger, C. Prognostic value of the CD4+/CD8+ ratio of tumour infiltrating lymphocytes in colorectal cancer and HLA-DR expression on tumour cells. *Cancer Immunol Immunother* **52**, 423-8 (2003).
6. Galon, J. *et al.* Towards the introduction of the 'Immunoscore' in the classification of malignant tumours. *J Pathol* **232**, 199-209 (2014).
7. Angell, H.K., Bruni, D., Barrett, J.C., Herbst, R. & Galon, J. The Immunoscore: Colon Cancer and Beyond. *Clin Cancer Res* **26**, 332-339 (2020).
8. Mlecnik, B. *et al.* Multicenter International Society for Immunotherapy of Cancer Study of the Consensus Immunoscore for the Prediction of Survival and Response to Chemotherapy in Stage III Colon Cancer. *J Clin Oncol* **38**, 3638-3651 (2020).
9. Buisseret, L. *et al.* Reliability of tumor-infiltrating lymphocyte and tertiary lymphoid structure assessment in human breast cancer. *Mod Pathol* **30**, 1204-1212 (2017).
10. Väyrynen, J.P. *et al.* An improved image analysis method for cell counting lends credibility to the prognostic significance of T cells in colorectal cancer. *Virchows Arch* **460**, 455-65 (2012).

bioRxiv preprint doi: https://doi.org/10.1101/2022.07.06.498984; this version posted July 7, 2022. The copyright holder for this preprint (which was not certified by peer review) is the author/funder, who has granted bioRxiv a license to display the preprint in perpetuity. It is made available under aCC-BY-NC 4.0 International license.

11. Diem, K. *et al.* Image analysis for accurately counting CD4+ and CD8+ T cells in human tissue. *J Virol Methods* **222**, 117-21 (2015).

12. Lu, Z. *et al.* Deep-Learning-Based Characterization of Tumor-Infiltrating Lymphocytes in Breast Cancers From Histopathology Images and Multiomics Data. *JCO Clin Cancer Inform* **4**, 480-490 (2020).

13. Saltz, J. *et al.* Spatial Organization and Molecular Correlation of Tumor-Infiltrating Lymphocytes Using Deep Learning on Pathology Images. *Cell Rep* **23**, 181-193.e7 (2018).

14. Amgad, M. *et al.* Report on computational assessment of Tumor Infiltrating Lymphocytes from the International Immuno-Oncology Biomarker Working Group. *NPJ Breast Cancer* **6**, 16 (2020).

15. Idos, G.E. *et al.* The Prognostic Implications of Tumor Infiltrating Lymphocytes in Colorectal Cancer: A Systematic Review and Meta-Analysis. *Sci Rep* **10**, 3360 (2020).

16. Baghban, R. *et al.* Tumor microenvironment complexity and therapeutic implications at a glance. *Cell Commun Signal* **18**, 59 (2020).

17. Boulter, L., Bullock, E., Mabruk, Z. & Brunton, V.G. The fibrotic and immune microenvironments as targetable drivers of metastasis. *Br J Cancer* **124**, 27-36 (2021).

18. Kather, J.N. *et al.* Predicting survival from colorectal cancer histology slides using deep learning: A retrospective multicenter study. *PLoS Med* **16**, e1002730 (2019).

19. Kather, J.N. *et al.* Topography of cancer-associated immune cells in human solid tumors. *Elife* **7**(2018).

20. Qi, L. *et al.* Identification of prognostic spatial organization features in colorectal cancer microenvironment using deep learning on histopathology images. *Medicine in Omics* **2**, 100008 (2021).

21. Yuan, Y. Modelling the spatial heterogeneity and molecular correlates of lymphocytic infiltration in triple-negative breast cancer. *J R Soc Interface* **12**(2015).

bioRxiv preprint doi: https://doi.org/10.1101/2022.07.06.498984; this version posted July 7, 2022. The copyright holder for this preprint (which was not certified by peer review) is the author/funder, who has granted bioRxiv a license to display the preprint in perpetuity. It is made available under aCC-BY-NC 4.0 International license.

22. Heindl, A. *et al.* Relevance of Spatial Heterogeneity of Immune Infiltration for Predicting Risk of Recurrence After Endocrine Therapy of ER+ Breast Cancer. *J Natl Cancer Inst* **110**(2018).

23. Ding, R. *et al.* Image analysis reveals molecularly distinct patterns of TILs in NSCLC associated with treatment outcome. *NPJ Precis Oncol* **6**, 33 (2022).

24. AbdulJabbar, K. *et al.* Geospatial immune variability illuminates differential evolution of lung adenocarcinoma. *Nat Med* **26**, 1054-1062 (2020).

25. Bilal, M. *et al.* Development and validation of a weakly supervised deep learning framework to predict the status of molecular pathways and key mutations in colorectal cancer from routine histology images: a retrospective study. *Lancet Digit Health* **3**, e763-e772 (2021).

26. Newman, A.M. *et al.* Robust enumeration of cell subsets from tissue expression profiles. *Nat Methods* **12**, 453-7 (2015).

27. Aran, D., Hu, Z. & Butte, A.J. xCell: digitally portraying the tissue cellular heterogeneity landscape. *Genome Biol* **18**, 220 (2017).

28. Jiménez-Sánchez, A., Cast, O. & Miller, M.L. Comprehensive Benchmarking and Integration of Tumor Microenvironment Cell Estimation Methods. *Cancer Res* **79**, 6238-6246 (2019).

29. Schmauch, B. *et al.* A deep learning model to predict RNA-Seq expression of tumours from whole slide images. *Nat Commun* **11**, 3877 (2020).

30. Huntington, N.D., Cursons, J. & Rautela, J. The cancer-natural killer cell immunity cycle. *Nat Rev Cancer* **20**, 437-454 (2020).

31. Liu, Y. *et al.* Comparative Molecular Analysis of Gastrointestinal Adenocarcinomas. *Cancer Cell* **33**, 721-735.e8 (2018).

32. Guinney, J. *et al.* The consensus molecular subtypes of colorectal cancer. *Nat Med* **21**, 1350-6 (2015).

bioRxiv preprint doi: https://doi.org/10.1101/2022.07.06.498984; this version posted July 7, 2022. The copyright holder for this preprint (which was not certified by peer review) is the author/funder, who has granted bioRxiv a license to display the preprint in perpetuity. It is made available under aCC-BY-NC 4.0 International license.

493 33. Davoli, T., Uno, H., Wooten, E.C. & Elledge, S.J. Tumor aneuploidy correlates with
494 markers of immune evasion and with reduced response to immunotherapy. *Science*
495 **355**(2017).
496 34. Mardis, E.R. Neoantigens and genome instability: impact on immunogenomic phenotypes
497 and immunotherapy response. *Genome Med* **11**, 71 (2019).
498 35. Boland, C.R. & Goel, A. Microsatellite instability in colorectal cancer. *Gastroenterology*
499 **138**, 2073-2087.e3 (2010).
500 36. Laidlaw, B.J., Craft, J.E. & Kaech, S.M. The multifaceted role of CD4(+) T cells in
501 CD8(+) T cell memory. *Nat Rev Immunol* **16**, 102-11 (2016).
502 37. Graham, S. *et al.* Hover-Net: Simultaneous segmentation and classification of nuclei in
503 multi-tissue histology images. *Med Image Anal* **58**, 101563 (2019).
504 38. Galon, J. & Bruni, D. Approaches to treat immune hot, altered and cold tumours with
505 combination immunotherapies. *Nat Rev Drug Discov* **18**, 197-218 (2019).
506 39. Halbrook, C.J., Pasca di Magliano, M. & Lyssiotis, C.A. Tumor cross-talk networks
507 promote growth and support immune evasion in pancreatic cancer. *Am J Physiol*
508 *Gastrointest Liver Physiol* **315**, G27-G35 (2018).
509 40. Chen, Z. *et al.* A Machine Learning Model to Predict the Triple Negative Breast Cancer
510 Immune Subtype. *Front Immunol* **12**, 749459 (2021).
511 41. Hu, J. *et al.* Using deep learning to predict anti-PD-1 response in melanoma and lung
512 cancer patients from histopathology images. *Transl Oncol* **14**, 100921 (2021).
513 42. Väyrynen, J.P. *et al.* Prognostic Significance of Immune Cell Populations Identified by
514 Machine Learning in Colorectal Cancer Using Routine Hematoxylin and Eosin-Stained
515 Sections. *Clin Cancer Res* **26**, 4326-4338 (2020).
516 43. Reichling, C. *et al.* Artificial intelligence-guided tissue analysis combined with immune
517 infiltrate assessment predicts stage III colon cancer outcomes in PETACC08 study. *Gut*
518 **69**, 681-690 (2020).

bioRxiv preprint doi: https://doi.org/10.1101/2022.07.06.498984; this version posted July 7, 2022. The copyright holder for this preprint (which was not certified by peer review) is the author/funder, who has granted bioRxiv a license to display the preprint in perpetuity. It is made available under aCC-BY-NC 4.0 International license.

519 44. Echle, A. *et al.* Clinical-Grade Detection of Microsatellite Instability in Colorectal Tumors
520 by Deep Learning. *Gastroenterology* **159**, 1406-1416.e11 (2020).
521 45. Kather, J.N. *et al.* Deep learning can predict microsatellite instability directly from
522 histology in gastrointestinal cancer. *Nat Med* **25**, 1054-1056 (2019).
523 46. Park, J.H., Richards, C.H., McMillan, D.C., Horgan, P.G. & Roxburgh, C.S.D. The
524 relationship between tumour stroma percentage, the tumour microenvironment and
525 survival in patients with primary operable colorectal cancer. *Ann Oncol* **25**, 644-651
526 (2014).
527 47. Li, Y. *et al.* Predicting tumor response to drugs based on gene-expression biomarkers of
528 sensitivity learned from cancer cell lines. *BMC Genomics* **22**, 272 (2021).
529 48. Macenko, M. *et al.* A method for normalizing histology slides for quantitative analysis. in
530 *2009 IEEE International Symposium on Biomedical Imaging: From Nano to Macro* 1107-
531 1110 (2009).
532 49. Deng, J. *et al.* ImageNet: A large-scale hierarchical image database. in *2009 IEEE*
533 *Conference on Computer Vision and Pattern Recognition* 248-255 (2009).
534 50. Failmezger, H. *et al.* Topological Tumor Graphs: A Graph-Based Spatial Model to Infer
535 Stromal Recruitment for Immunosuppression in Melanoma Histology. *Cancer Res* **80**,
536 1199-1209 (2020).
537 51. Lee, H.O. *et al.* Lineage-dependent gene expression programs influence the immune
538 landscape of colorectal cancer. *Nat Genet* **52**, 594-603 (2020).
539 52. Wolf, F.A., Angerer, P. & Theis, F.J. SCANPY: large-scale single-cell gene expression
540 data analysis. *Genome Biol* **19**, 15 (2018).
541 53. Palla, G. *et al.* Squidpy: a scalable framework for spatial omics analysis. *Nat Methods* **19**,
542 171-178 (2022).
543
544

bioRxiv preprint doi: https://doi.org/10.1101/2022.07.06.498984; this version posted July 7, 2022. The copyright holder for this preprint (which was not certified by peer review) is the author/funder, who has granted bioRxiv a license to display the preprint in perpetuity. It is made available under aCC-BY-NC 4.0 International license.

545 **FIGURES**

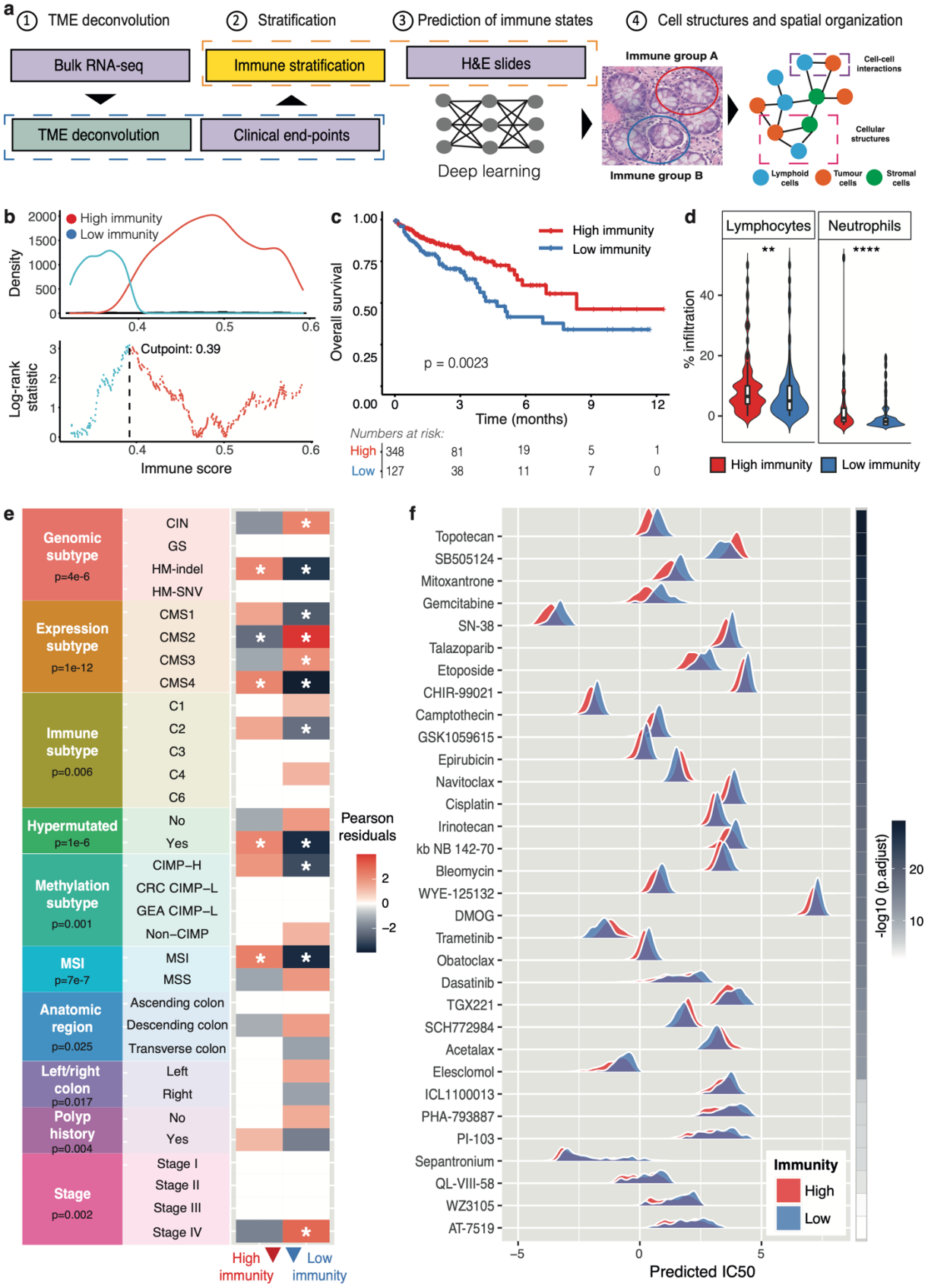

546

547 **Figure 1. Study workflow and immunity-based stratification of colon adenocarcinoma. (a)**

548 Workflow of the study. A prognostic classifier of colon adenocarcinoma was defined based on

bioRxiv preprint doi: https://doi.org/10.1101/2022.07.06.498984; this version posted July 7, 2022. The copyright holder for this preprint (which was not certified by peer review) is the author/funder, who has granted bioRxiv a license to display the preprint in perpetuity. It is made available under aCC-BY-NC 4.0 International license.

549 RNA-seq inferred immune activity in the tumours. An H&E based deep learning classifier was
550 then on these labels, and differences in cellular compositions and interactions between the two
551 groups were subsequently described. **(b)** Optimisation of tumour immunity threshold to maximise
552 survival differences. The dotted line highlights the optimal cut-point of 0.39. **(c)** The high and low
553 immunity groups defined using the cut-off in (b) show significantly different overall survival in
554 the TCGA-COAD cohort. (d) The high immunity group presents higher fractions of lymphocytes
555 and neutrophils, as scored by pathologists. (e) Differences in colon adenocarcinoma molecular
556 subgroup and clinical characteristics between high and low immunity tumours, inferred from
557 conditional independence tests. Only significantly associated characteristics are shown. The stars
558 mark Pearson residuals greater than 2 or less than -2, indicating the strongest correlations. **(f)**
559 Predicted drug sensitivity of TCGA-COAD tumours to a variety of anti-cancer compounds,
560 compared between high and low immunity groups. Only compounds showing significant
561 differences in drug sensitivity are shown (ranked by the magnitude of the difference).
562
563

bioRxiv preprint doi: https://doi.org/10.1101/2022.07.06.498984; this version posted July 7, 2022. The copyright holder for this preprint (which was not certified by peer review) is the author/funder, who has granted bioRxiv a license to display the preprint in perpetuity. It is made available under aCC-BY-NC 4.0 International license.

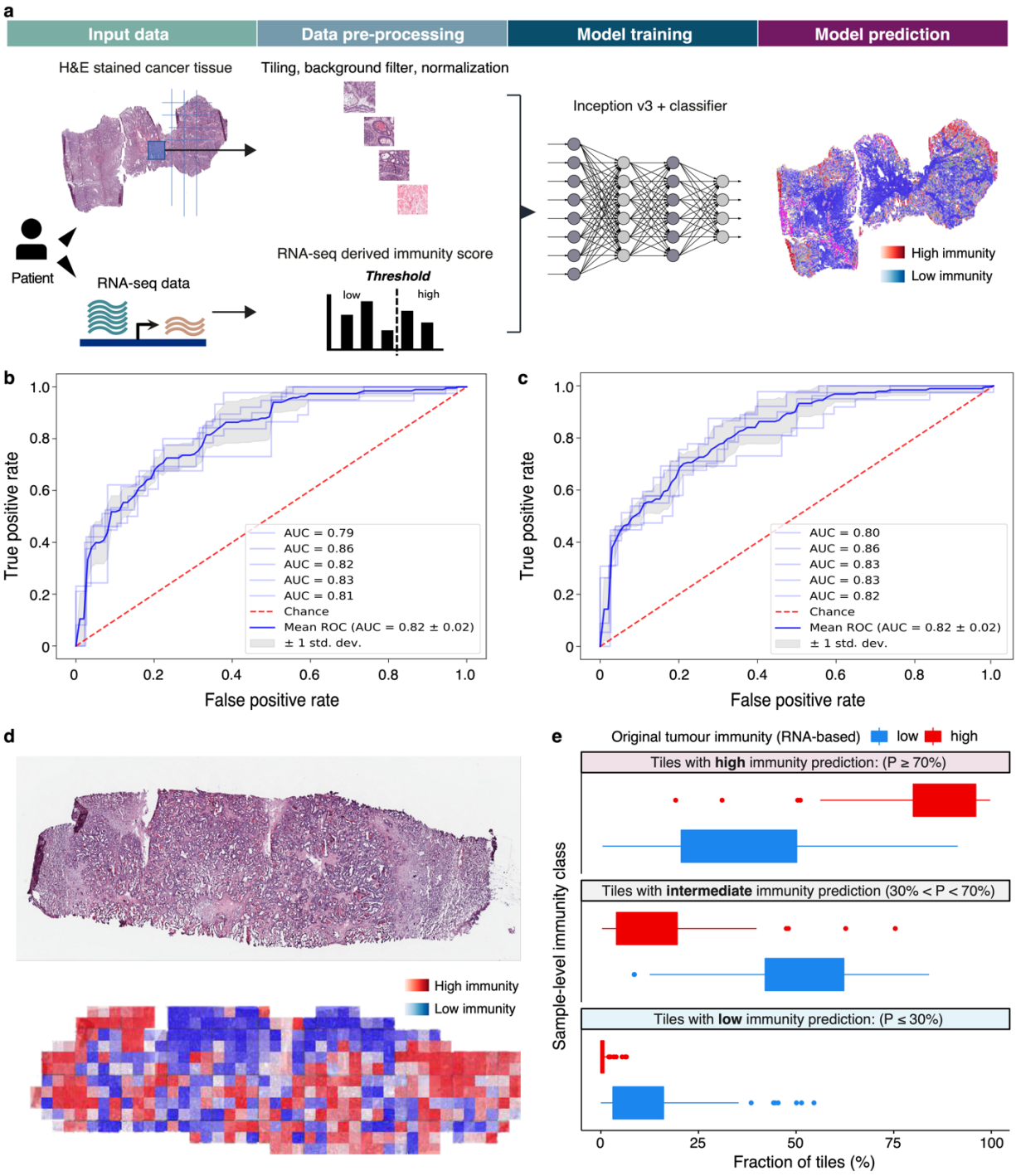

Figure 2. Deep learning classifier of tumour immunity. (a) Pipeline for the identification of RNA-seq based immune phenotypes in digital images of H&E stained cancer tissue. (b-c) A mean accuracy (AUC) of 82% is obtained when predicting the immune phenotype of colon cancer H&E slides with 5-fold cross validation by averaging the probability per tile (b) and counting the percentage of tiles (c), respectively. (d) Example of an H&E stained slide (top) and the corresponding immunity predictions of the model within the same slide (bottom). The colour gradient from blue to red reflects increasing probability of high immune content in each patch. (e)

bioRxiv preprint doi: https://doi.org/10.1101/2022.07.06.498984; this version posted July 7, 2022. The copyright holder for this preprint (which was not certified by peer review) is the author/funder, who has granted bioRxiv a license to display the preprint in perpetuity. It is made available under aCC-BY-NC 4.0 International license.

572 Immunity class deep learning predictions in each tile, compared between samples with high and
573 low overall immunity (as inferred from RNA-seq data). Tile-level predictions have been classed
574 as high, intermediate or low immunity based on the probability of belonging to the HI/LI group
575 as indicated.
576

bioRxiv preprint doi: https://doi.org/10.1101/2022.07.06.498984; this version posted July 7, 2022. The copyright holder for this preprint (which was not certified by peer review) is the author/funder, who has granted bioRxiv a license to display the preprint in perpetuity. It is made available under aCC-BY-NC 4.0 International license.

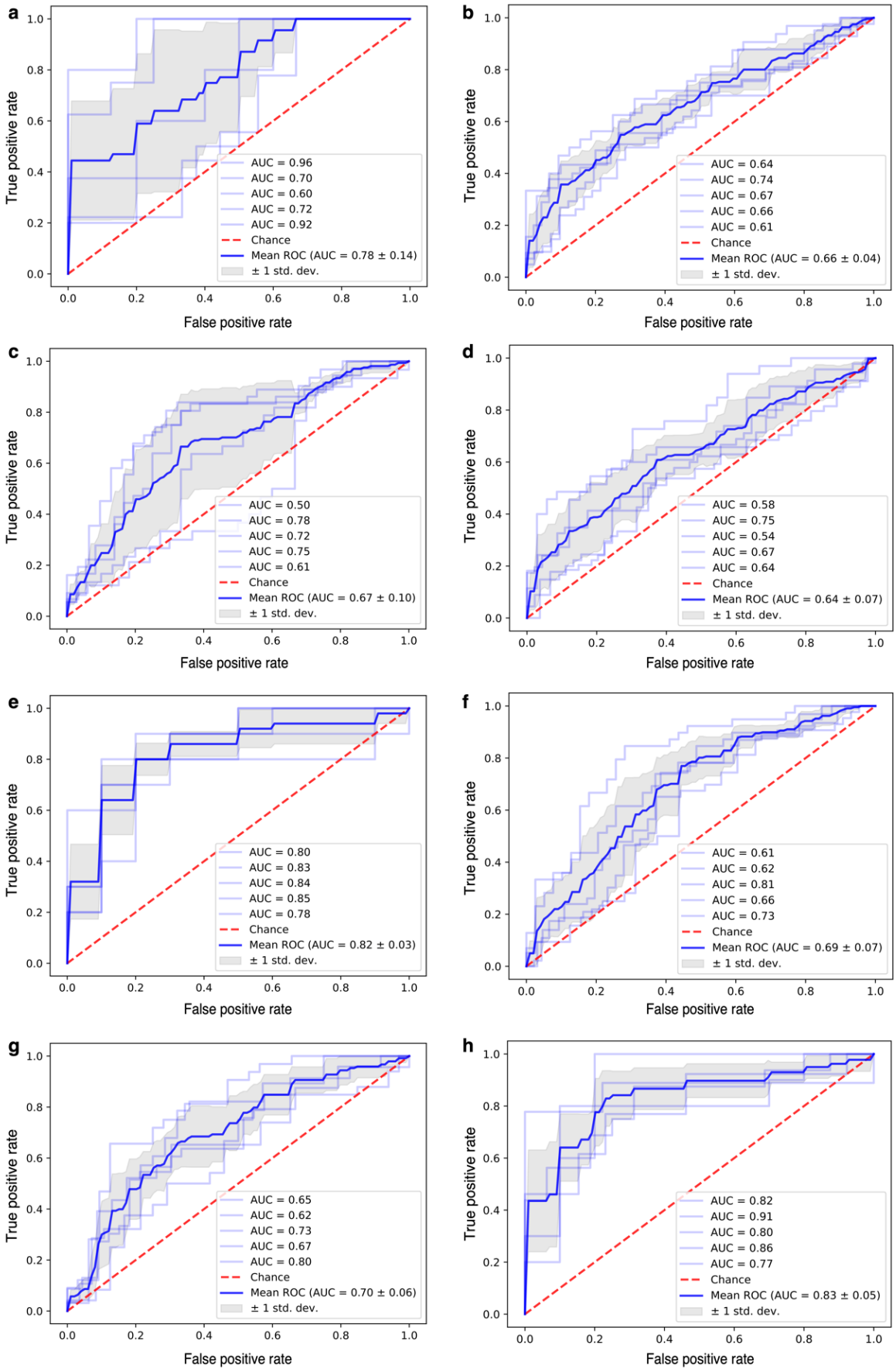

577

578 **Figure 3. Prediction of the subgroups of CD4+ and CD8+ T cells in H&E images.** Mean

579 accuracies (AUC) are shown for predictions of each of the following T cell categories: (a) generic

bioRxiv preprint doi: https://doi.org/10.1101/2022.07.06.498984; this version posted July 7, 2022. The copyright holder for this preprint (which was not certified by peer review) is the author/funder, who has granted bioRxiv a license to display the preprint in perpetuity. It is made available under aCC-BY-NC 4.0 International license.

580 CD4+ T cells - 78%; (b) generic CD8+ T cells - 66%; (c) CD4+ naïve T cells - 67%; (d) CD8+

581 naïve T cells – 64%; (e) CD4+ central memory T cells - 82%; (f) CD8+ central memory T cells -

582 69%; (g) CD4+ effector memory T cells - 70%; (h) CD8+ effector memory T cells - 83%.

583

584

bioRxiv preprint doi: https://doi.org/10.1101/2022.07.06.498984; this version posted July 7, 2022. The copyright holder for this preprint (which was not certified by peer review) is the author/funder, who has granted bioRxiv a license to display the preprint in perpetuity. It is made available under aCC-BY-NC 4.0 International license.

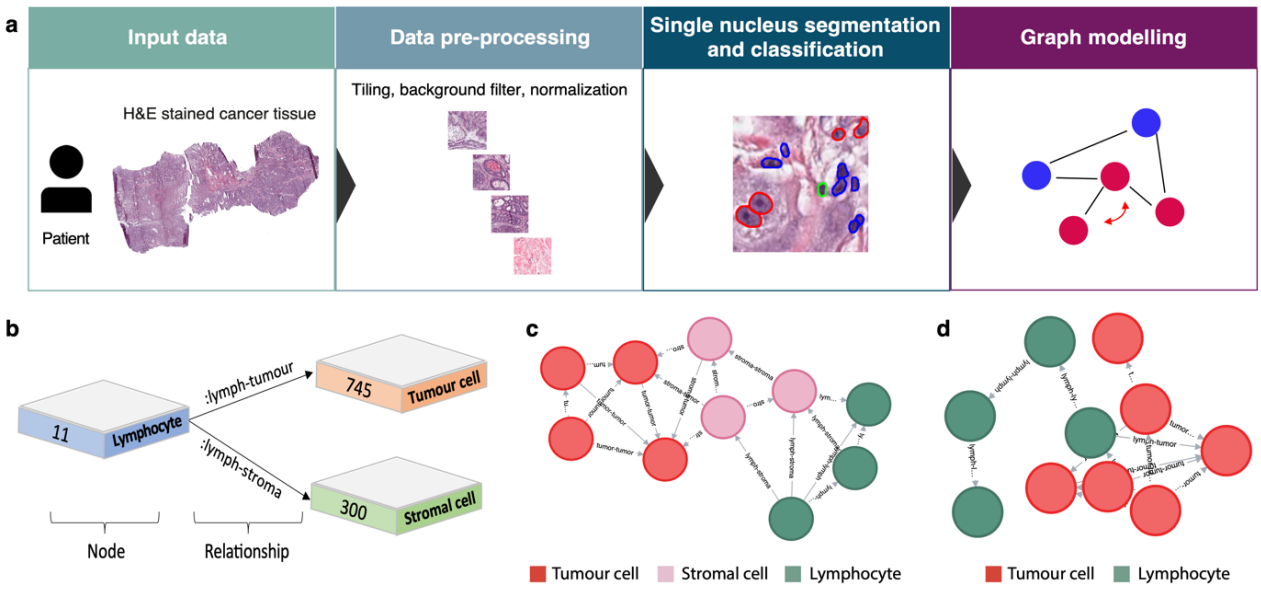

585

586 **Figure 4. Graph analysis of the cellular organisation of the immune response in colon**
587 **adenocarcinoma.** (a) Pipeline of the graph analysis approach. After preprocessing the WSIs, cells
588 are segmented and classified using HoVer-Net, following further graph modelling and storage.
589 (b) The inferred cell-cell interactions within the tissue are stored in a Neo4j graph database for
590 further analysis. The database structure is shown, with representative relationships between cell
591 types illustrated. (c) Example of a stromal barrier graph structure, separating tumour cells from
592 lymphocytes. (d) Example of a graph structure illustrating lymphocyte infiltration of the tumour.

593

594

595

596

597

bioRxiv preprint doi: https://doi.org/10.1101/2022.07.06.498984; this version posted July 7, 2022. The copyright holder for this preprint (which was not certified by peer review) is the author/funder, who has granted bioRxiv a license to display the preprint in perpetuity. It is made available under aCC-BY-NC 4.0 International license.

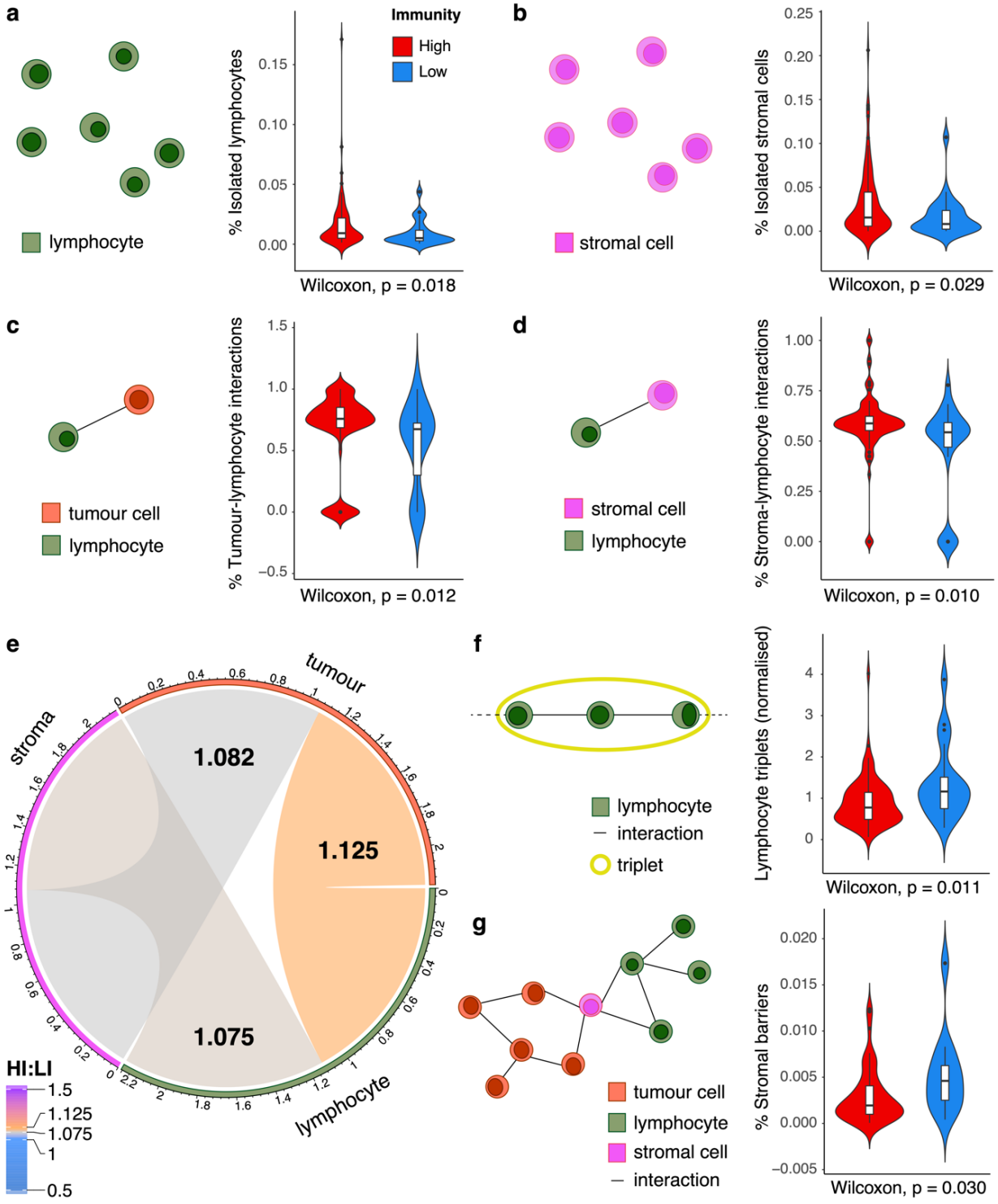

Figure 5. Cellular organization differences in high versus low immunity tumours. High (red) and low (blue) immunity groups are compared in terms of: (a) the fraction of isolated lymphocytes; (b) the fraction of isolated stromal cells; (c) the fraction of direct tumour-lymphocyte interactions; (d) the fraction of direct stroma-lymphocyte interactions. (e) The fold change in interactions established between pairs of cell types in high versus low immunity tumours. The ratio of median numbers in either group is depicted. (f) Fraction of lymphocyte

bioRxiv preprint doi: https://doi.org/10.1101/2022.07.06.498984; this version posted July 7, 2022. The copyright holder for this preprint (which was not certified by peer review) is the author/funder, who has granted bioRxiv a license to display the preprint in perpetuity. It is made available under aCC-BY-NC 4.0 International license.

605 triples compared between high and low immunity samples containing at least one such structure.
606 (g) Fraction of stromal barriers compared between high and low immunity samples containing at
607 least one such structure. Schematic depictions of cellular structures are displayed alongside each
608 comparison.
609

bioRxiv preprint doi: https://doi.org/10.1101/2022.07.06.498984; this version posted July 7, 2022. The copyright holder for this preprint (which was not certified by peer review) is the author/funder, who has granted bioRxiv a license to display the preprint in perpetuity. It is made available under aCC-BY-NC 4.0 International license.

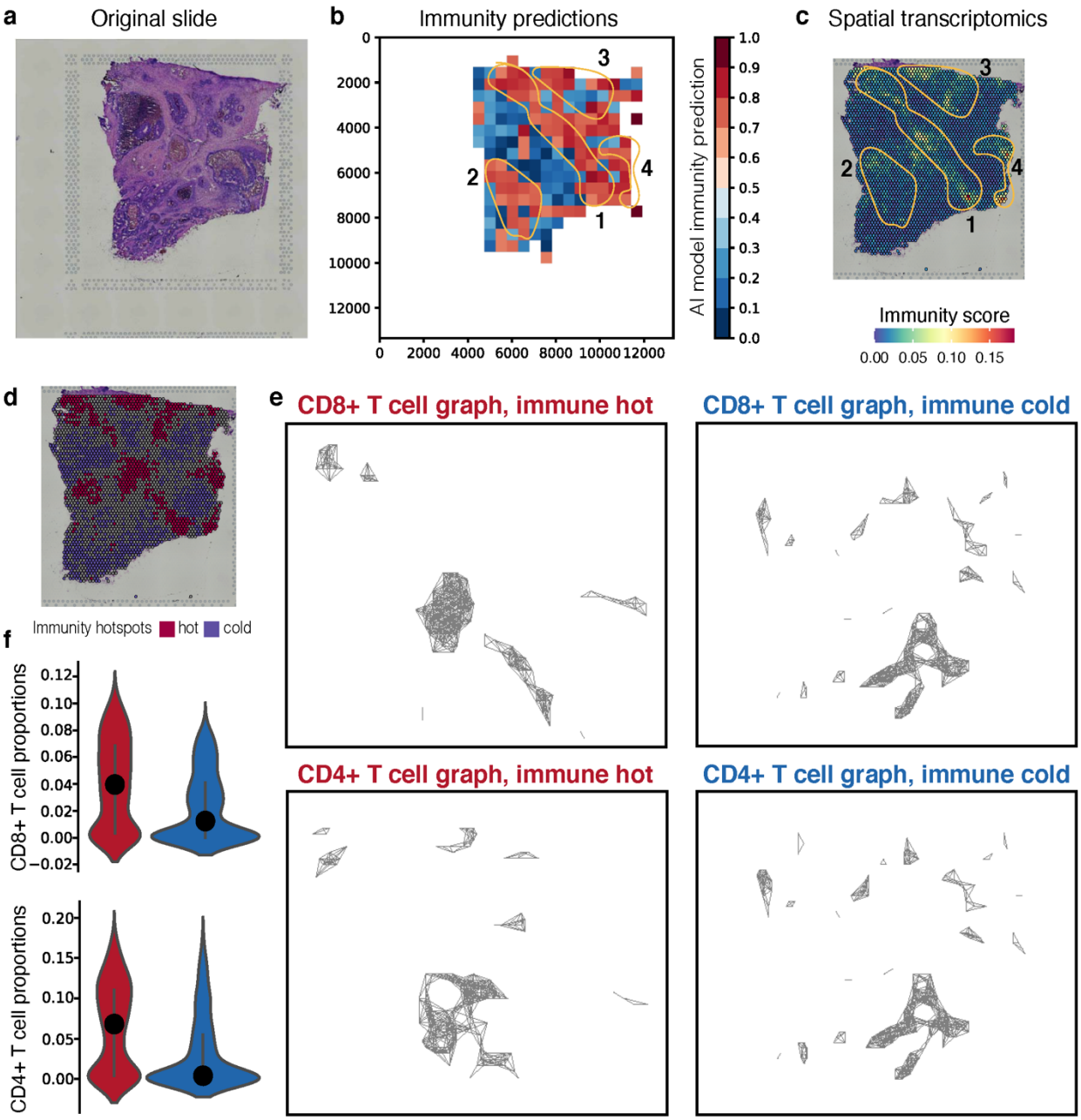

Figure 6. Validation of AI model predictions using spatial transcriptomics data. (a) Original colorectal tissue slide employed for spatial transcriptomics from Visium. (b) The immunity prediction of the deep learning model on H&E staining-derived patches. Red indicates areas of high immunity, blue indicates low immunity. Four high immunity islands are indicated with an orange outline and numbered 1-4. (c) Immunity score across spatial transcriptomics spots. Red and yellow areas indicate high immunity, and the same islands 1-4 as in (c) are indicated on the slide. (d) Immune hot (red) and cold (blue) hotspots defined from spatial transcriptomics. The grey spots have intermediate levels and cannot be classed in either group. (e) CD8+ (top) and

bioRxiv preprint doi: https://doi.org/10.1101/2022.07.06.498984; this version posted July 7, 2022. The copyright holder for this preprint (which was not certified by peer review) is the author/funder, who has granted bioRxiv a license to display the preprint in perpetuity. It is made available under aCC-BY-NC 4.0 International license.

619 CD4+ (bottom) T cell interaction graphs within hot (left) and cold (right) immunity areas. (f)
620 CD8+ (top) and CD4+ (bottom) T cell proportions compared between immune hot (red) and cold
621 (blue) graphs.
622